Translational Oncology 14 (2021) 101167

Contents lists available at ScienceDirect

Translational Oncology

journal homepage: www.elsevier.com/locate/tranon

Original Research

MTA2 sensitizes gastric cancer cells to PARP inhibition by induction of DNA replication stress

Jinwen Shi [a], Xiaofeng Zhang [a], Jin'e Li [a], Wenwen Huang [b], Yini Wang [a], Yi Wang [a], Jun Qin [a,*]

[a] State Key Laboratory of Proteomics, Beijing Proteome Research Center, National Center for Protein Sciences (Beijing), Beijing Institute of Lifeomics, Beijing 102206, China

[b] State Key Laboratory of Oncology in South China, Collaborative Innovation Center for Cancer Medicine, Sun Yat-sen University Cancer Center, Sun Yat-sen University, Guangzhou 510060, China

ARTICLE INFO

Keywords:
MTA2
Olaparib
Gastric cancer
Replication stress
Replication origins

ABSTRACT

Poly (ADP-ribose) polymerase (PARP) inhibitor olaparib selectively kills cancer cells with BRCA-deficiency and is approved for BRCA-mutated breast, ovarian and pancreatic cancers by FDA. However, phase III study of olaparib failed to show a significant improvement in overall survival in patients with gastric cancer (GC). To discover an effective biomarker for GC patient-selection in olaparib treatment, we analyzed proteomic profiling of 12 GC cell lines. MTA2 was identified to confer sensitivity to olaparib by aggravating olaparib-induced replication stress in cancer cells. Mechanistically, we applied Cleavage Under Targets and Tagmentation assay to find that MTA2 proteins preferentially bind regions of replication origin-associated DNA sequences, which could be enhanced by olaparib treatment. Furthermore, MTA2 was validated here to render cancer cells susceptible to combination of olaparib with ATR inhibitor AZD6738. In general, our study identified MTA2 as a potential biomarker for olaparib sensitivity by aggravating olaparib-induced replication stress.

1. Introduction

Gastric cancer (GC) is the third leading cause of cancer death and the fifth most common malignancy worldwide, over 1 million new cases of gastric cancer were diagnosed in 2018 [1]. Complete surgical resection is the only potential cure for gastric cancer, however, prognosis after curative resection integrated with neoadjuvant and adjuvant therapies remains poor that 5 years overall survival is less than 30% and median overall survival in metastatic patients is of 1 year, it is mainly because of high rate of recurrence and low efficacy of adjuvant therapy [2].

Currently, chemotherapy is still the main approach for treatment of patients with advanced metastatic GC, even though targeted and immune therapies have entered the therapeutic field. Trastuzumab is the only molecularly targeted drug approved in first-line therapy for the treatment of patients with HER2-overexpressing GC, while there are only 15–37% of GCs exhibiting elevated HER2 expression [3]. For HER2-negative patients, chemotherapy remains standard treatment including single drug or multidrug combination of platinum, fluoropyrimidine and paclitaxel compounds. Despite multiple cytotoxic drugs as options, only 40% of patients who developed resistance to first-line chemotherapy are susceptible to second-line chemotherapy on progression [4]. The other approved targeted drugs are VEGFR-2 antagonists ramucirumab and apatinib used respectively as second-line and third-line treatment, at present, few targeted therapies are still available for metastatic GC. As for immunotherapy, pembrolizumab and nivolumab has been approved as third-line treatment for patients with GC in USA and East Asia respectively. Altogether, the limited options in the treatment of GC make it particularly important to find and incorporate more therapeutic targets and drugs into the scope of clinical treatment.

Poly (ADP-ribose) polymerase (PARP) family is a group of enzymes involved in DNA damage response (DDR)(5). The main function of these enzymes is to recruit DNA repair proteins to the damaged sites through catalyzing ADP-ribosylation and leading to formation of poly (ADP-ribose) polymers [6]. PARP1 is the most abundant member in this family and shares similar roles in DDR processes with PARP2 [5]. Since two

Grant support: This work was supported by the National Key Research and Development Program of China (2017YFC0908404, 2018YFA0507503, 2017YFA0505102, 2017YFA0505103, 2017YFA0505104), National Natural Science Foundation of China (81874237, 31870828), Guangdong Key-Area R&D Program (2019B020229002), Guangzhou Science and Technology Program (201902020009).

* Corresponding author.
E-mail address: jqin1965@126.com (J. Qin).

https://doi.org/10.1016/j.tranon.2021.101167
Received 24 June 2021; Accepted 28 June 2021

back-to-back publications in 2005 that demonstrated the synthetic lethality of PARP1/2 inhibition in BRCA-deficient tumor [7,8], the race has been on to develop PARP inhibitors for cancer treatment [9].

PARP inhibitors have been approved for a variety of cancers and are undergoing multiple further preclinical and clinical researches for expanding indications including GC. As the first approved PARP inhibitor, in 2014, olaparib was approved by EMA in maintenance therapy of patients with BRCA-mutant ovarian cancer and received accelerated FDA approval in treatment of advanced-stage, BRCA-mutant ovarian cancers. Following approval for olaparib used in ovarian cancer treatment, rucaparib, niraparib and talazoparib are successively approved by FDA [10], currently these four PARP inhibitors are used as monotherapy in patients with various BRCA-mutant cancers, including ovarian, breast, prostate and pancreatic cancers [9]. Additionally, many clinical trials of PARP inhibitors for other cancers are carried out, such as: breast, lung, colorectal, gastric, liver and cervical cancer [11–16].

Overall survival of patients with metastatic GC was significantly improved by PARPi olaparib in combination with paclitaxel compared with placebo with paclitaxel in phase II trial [17], however, in phase III study, it failed to demonstrate a clinical benefit in advanced GC either in overall or ATM-negative population [14]. This is partly because an appropriate biomarker has not been selected in clinical trials that ATM-negative population might have been too small to determine a difference between treatment groups, and thus effective biomarkers with high frequency in GC population are needed. Currently, proteomics has becoming a promising technology that could enable insight to disease at the protein level and discover biomarkers to assist in selection of patients with potential benefit of drugs [18,19].

Here, we set out to discover biomarker to predict the sensitivity of GC cells to olaparib by proteomics approach and to explore its efficiency and molecular mechanism using in vivo and in vitro models. We applied label-free quantitative proteomics approach to 12 GC cell lines and collected indicated IC50 of these cell lines to olaparib. After correlation analysis and difference analysis, metastasis-associated protein 2 (MTA2) was identified as a potential biomarker with high frequency in GC tumor tissues. Following validation of MTA2 efficiency, exploration of biological mechanism was conducted by cell cycle analysis, interaction proteomics and CUT&Tags approach along with DNA sequencing.

2. Materials and methods

2.1. Gastric cancer cell culture and drug treatment

The 12 human gastric cancer cell lines used in this study are listed in Fig. 1B and Fig S1A. MKN45 and AGS cell lines were purchased from Institute of Basic Medical Sciences of the Chinese Academy of Medical Sciences, KATO III and SNU1 were purchased from Shanghai Institute of Biomedical Sciences of the Chinese Academy of Sciences, and the rest 8

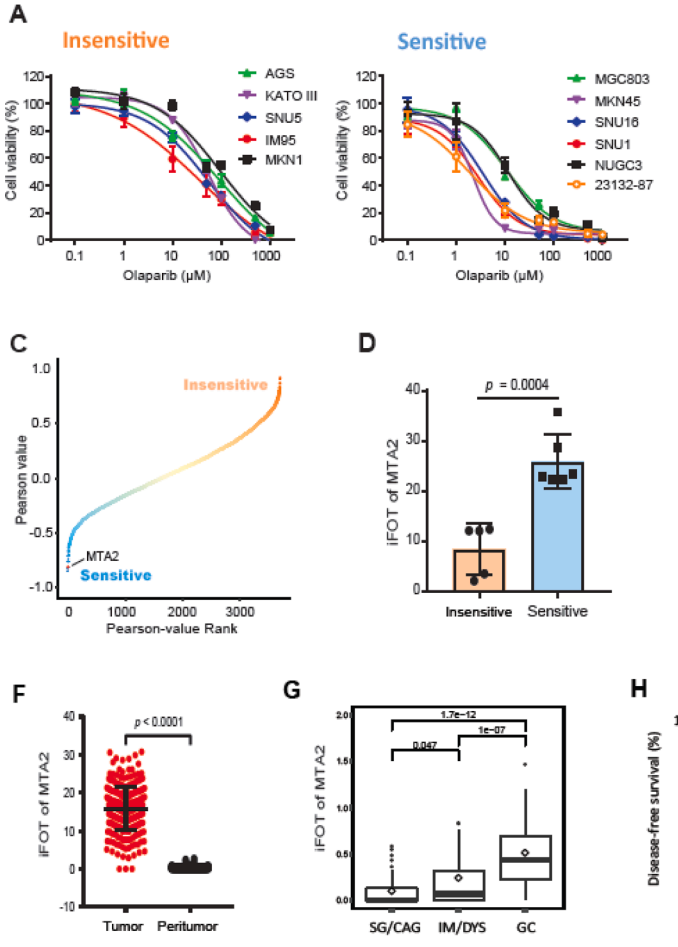

Fig. 1. MTA2 protein level is positively correlated with the GC cell sensitivity to PARP inhibitor and it overexpresses along with progress of GC. A The sensitivity of eleven GC cell lines to olaparib. Twelve gastric cancer cell lines were treated with olaparib at indicated concentration. Cells were measured by WST assay. Based on the sensitivity to olaparib, the cells were classified into two groups. MKN74 with IC50 greater than 100 μM was excluded. Data are presented as mean ± SD. B Grouping of olaparib-sensitive and -insensitive cell proteomes by PCA. Component 1 accounts for 10.19% of total data variability and component 2 accounts for 8.68%. C Pearson correlation analysis of each protein level with cell sensitivity to olaparib. Pearson-value rank was plotted against Pearson value. Proteins with a detection frequency of lower than 50% in the cell proteome or lower than 20% in our own clinical proteome of gastric cancer were excluded. The level of each remaining protein was obtained by calculating the average value of FOT in 11 cells. IC50 of olaparib was calculated from the WST assays. MTA2 is highlighted in red. D Comparison of MTA2 protein levels in olaparib-sensitive cells and olaparib insensitive cells. Statistical significance of the difference was analyzed using two-tailed unpaired Student's t tests. E Pearson's correlation analysis between sensitivity to olaparib and MTA2 protein level. *P*-Value of Pearson's correlation was calculated by R function cor.test. F FOT of MTA2 in 300 pairs of gastric tumors and nearby tissues. G FOT of MTA2 in superficial gastritis (SG)/chronic atrophic gastritis (CAG), intestinal metaplasia (IM)/ dysplasia (DYS) and gastric cancer (GC) tissues. H Kaplan–Meier survival analysis of disease-free survival based on the ratio of MTA2 protein level in tumor to the nearby tissue (T/P ratio) in the proteomics dataset. Patients with the highest MTA2 T/P ratio (n = 218) are compared to the lower individuals (n = 82). *P*-value is determined by log-rank test.

cell lines were purchased from Cobioer Biosciences Co., Ltd (Nanjing, Jiangsu, China). All cell lines were verified by short random sequence (STR) analysis. NUGC3, MKN45, SNU16, AGS, MGC803, SNU1, MKN1, MKN74 and HGC27 were cultured in RPMI 1640 medium (Gibco, USA) supplemented with 10% FBS (Gibco, USA) and 1% penicillin/streptomycin (Gibco, USA); KATOIII and SNU5 were cultured in IMDM medium (Gibco, USA) supplemented with 20% FBS (Gibco, USA) and 1% penicillin/streptomycin (Gibco, USA); IM95 were grown in high glucose DMEM medium (Gibco, USA) containing 10% FBS (Gibco, USA), 1% penicillin/streptomycin (Gibco, USA) and 10 μg/mL insulin-transferrin selenium (Gibco, USA). Cells were treated with indicated concentrations of following drugs: olaparib (MedChem Express, USA) and ceralasertib (MedChem Express, USA).

2.2. Stable cell lines and RNAi

All shRNAs subcloned into pLKO.1 plasmid were purchased from Amogene (Xiamen, Fujian, China). The MTA2 shRNA target sequence is GCACCAAUGAGCCUAUUGUTT. An shGFP sequence was used as a control. To generate lentivirus expression plasmid, we subcloned MTA2 full length cDNA into a pLVX-SBP-Flag vector. Lentiviral particles were generated in HEK293T cells and gastric cancer cells were infected according to Addgene's Lentivirus Production protocol.

All siRNA transfections were performed using Lipofectamine RNAiMAX (Invitrogen, USA) according to the manufacturer's instructions. The MTA2 and control siRNA duplexes were purchased from GenePharma (Suzhou, Jiangsu, China), their sequences were as follows:

MTA2-siRNA#1: 5′-CAGCCUGGCUGAUAGUAAUTT −3′
MTA2-siRNA#2: 5′-GCACCAAUGAGCCUAUUGUTT −3′
MTA2-siRNA#3: 5′-GGUGGGAGAUUACGUCUAUTT −3′
Non-targeting control siRNA: UUCUCCGAACGUGUCACGUTT

2.3. Cell viability assay

The sensitivity of cells to olaparib and ceralasertib was assessed by Cell Counting Kit-8 (MedChem Express, USA). Cells were plated in 96-well plates at 1500–4000 cells/well and cultured at 37 °C overnight for adhesion. After drug treatment, Cell Counting Kit-8 reagent was added to 10% and incubated for 1.5 h at 37 °C before reading the absorbance at 450 nm on a plate reader. Half-maximal inhibitory concentration (IC50) was determined using GraphPad Prism 7 software (GraphPad Software Inc., USA).

Wild type or MTA2-knockdown NUGC3 cells were plated at 1000-cells/well density in six-well plates and treated with indicated concentrations of olaparib. Cells were then grown at 37 °C for 14 days to allow colonies to form. Colonies were fixed with pre-chilled methanol and stained with 0.5% crystal violet in 70% methanol. Stained colonies were counted and statistical data were analyzed by *t*-test analysis.

2.4. Cell sample preparation for MS analysis

Cells were washed for three times with prechilled PBS and then collected. Lysis was then carried out in 1% sodium deoxycholate, 10 mM Tris(2-carboxyethyl) phosphine, 40 mM 2-chloroacetamide and 100 mM Tris–HCl pH8.5 at 95 °C for 5 min and by 5 min sonication (3 s on and 3 s off, amplitude 25%). After 16,000 g centrifugation at 4 °C for 10 min, 100 μg proteins in the cleared lysate were digested overnight with 1:50 trypsin (Promega, USA). The next day, digestion was stopped by adding 1% formic acid. Precipitated sodium deoxycholate was removed by 10 min 16,000 g centrifugation at 4 °C and peptides in supernatant were desalted on C_{18} StageTips. Desalted peptides were vacuum-dried and stored at –80 °C until subsequent LC-MS/MS analysis.

2.5. LC-MS/MS analysis

For LC-MS/MS analysis, a Fusion mass spectrometer (Thermo Fisher Scientific) was coupled on-line to an Easy-nLC 1000 HPLC nanoflow system (Thermo Fisher Scientific). The vacuum-dried peptides redissolved in 0.1% formic acid were loaded onto an in-house packed reversed-phase C_{18} precolumn (2 cm × 100 μm; particle size, 3 μm; pore size, 120 Å) and then separated by a 150 μm × 30 cm silica microcolumn (homemade; particle size, 1.9 μm; pore size, 120 Å) with a linear gradient of 6–40% Mobile Phase B (acetonitrile and 0.1% formic acid) at a flow rate of 600 nl/min for 150 min. To acquire mass spectra, data-dependent mode was applied by carrying out a Full MS scan (AGC target 3×10^6 ions, maximum injection time 20 ms, 300–1400 *m/z*, $R =$ 60,000 at 200 *m/z*) followed by up to 20 tandem MS/MS scans with high-energy collision dissociation (target 2×10^3 ions, max injection time 40 ms, isolation window 1.6 *m/z*, normalized collision energy of 27%), detected in the Iontrap (R = 15,000 at 200 *m/z*). Dynamic exclusion time was set to 18 s. All data was acquired using the Xcalibur software (Thermo Fisher Scientific).

2.6. Western blot analysis

Cells were washed with prechilled PBS and harvested into lysis buffer (150 mM NaCl, 10% glycerol, 0.3% Triton X-100, 50 mM Tris pH 8.0). Proteins were resolved via SDS-PAGE and transferred to PVDF membrane. Immunoblotting was performed with the following antibodies anti-MTA2 (ab8106, Abcam, Cambridge, UK, 1:1000), anti-CHK1 (ab40866, Abcam, Cambridge, UK, 1:200), anti-CHK1 pS345 (#2348, Cell Signaling Technology, MA, USA, 1:1000), anti-CHK1 pS317 (ab59239, Abcam, Cambridge, UK, 1:1000), anti-RPA32 (sc-56,770, Santa Cruz, CA, USA, 1:1000), anti-RPA32 pT21 (ab109394, Abcam, Cambridge, UK, 1:5000), anti-γH2AX (sc-517,348, Santa Cruz, CA, USA, 1:1000), anti-β-actin (#3700, Cell Signaling Technology, MA, USA, 1:1000), anti-rabbit IgG, HRP-linked (ZB-2301, ORIGENE, China, 1:10,000), anti-mouse IgG, HRP-linked (ZB-2305, ORIGENE, China, 1:10,000), and detected using enhanced chemiluminescence reagent (CWBIO, Beijing, China).

2.7. Affinity purification and mass spectrometry

Affinity purification coupled to mass spectrometry was performed as described previously [20] except following exceptions. After lysis in RIPA buffer and sonification, cells stably expressing Flag-MTA2 or control cells were centrifugated for 10 min at 9600 g. Additionally, after incubation with anti-Flag antibody, protein lysates were cleared by 9200 g centrifugation for 5 min.

2.8. Cell cycle analysis

Cell cycle analysis was performed using Cell Cycle and Apoptosis Analysis kit (Beyotime, China) according to the manufacturer's instructions. Briefly, cells were washed with cold PBS and fixed with prechilled 70% ethanol at 4 °C overnight. The next day, fixed cells were washed with PBS once and then labelled at 37 °C for 30 min with staining buffer containing 10 μg/ml propidium iodide and 5 μg/ml RNase A. Stained cells were detected immediately on flow cytometer (BD LSR Fortessa SORP) and acquired data was analyzed using the ModFit LT software.

2.9. CUT&Tag and data analysis

CUT&Tag assay was performed using HyperactiveTM In-Situ ChIP Library Prep Kit for Illumina (Vazyme Biotech, China) according to producer's instruction. Briefly, MKN45 cells were harvested, counted and centrifuged for 3 min at 600 × *g* at room temperature. Pellets of 1×10^5 cells were collected and washed with 500 μl Wash Buffer (20 mM

HEPES pH 7.5, 150 mM NaCl, 0.5 mM Spermidine (Sigma-Aldrich), 1 × Protease inhibitor cocktail (Sigma-Aldrich)), followed by 600 g centrifugation for 3 min at room temperature. Cell pellets were resuspended with 100 µl Wash Buffer. Concanavalin A-coated magnetic beads were prepared as 10 µl per sample as needed and washed twice with Binding Buffer (20 mM HEPES pH 7.5, 10 mM KCl, 1 mM MnCl2, 1 mM CaCl2). Subsequently, activated beads were added to resuspended cells and incubated at room temperature for 5–10 min. Next, unbound cells were removed after solution turned clear in the magnetic separation rack and the bead-bound cells were resuspended in 50 µl Antibody Buffer (20 mM HEPES pH 7.5, 150 mM NaCl, 0.5 mM Spermidine, 0.05% Digitonin, 2 mM EDTA, 0.1% BSA, 1 × Protease inhibitor cocktail). Then, 1 µg primary rabbit monoclonal anti-MTA2 antibody (ab8106, Abcam, Cambridge, UK) or normal rabbit IgG (ZDR-5003, ZDGB-BIO, China) was added and incubated 2 h at room temperature with gentle rotation. Following removing primary antibody supernatant after standing in the magnetic separation rack, 1 µg secondary goat anti-rabbit IgG H&L (ZDR-5118, ZDGB-BIO, China) diluted in 50µl of Dig-wash buffer (20 mM HEPES pH 7.5, 150 mM NaCl, 0.5 mM Spermidine, 0.05% Digitonin, 1 × Protease inhibitor cocktail) was added in cells and incubated at room temperature for 30–60 min. Cells were then washed with 800 µl Dig-wash buffer three times. The Hyperactive pA-Tn5 Transposase was diluted using Dig-300 Buffer (20 mM HEPES pH 7.5, 300 mM NaCl, 0.5 mM Spermidine, 0.01% Digitonin, 1 × Protease inhibitor cocktail) and incubated with cells at room temperature for 1 h. Following incubation and three times washing with Dig-300 Buffer, cells were then resuspended in 300 µl Tagmentation Buffer (10 mM $MgCl_2$ in Dig-300 buffer) and incubated at 37 °C for 1 h. To terminate tagmentation, 10 µl of 0.5 M EDTA, 3 µl 10% SDS and 2.5 µl of 20 mg/ml Proteinase K were added and incubated at 50 °C for 1 h. Phenol-chloroform-isoamyl alcohol extraction and ethanol precipitation were used to purify DNA. To amplify library, 24 µl DNA was mixed with 1 µl TruePrep Amplify Enzyme (Vazyme Biotech, China), 10 µl 5 × TruePrep Amplify Enzyme Buffer, 5 µl ddH2O, and 5 µl uniquely barcoded i5 and i7 primers from TruePrep Index Kit V2 for Illumina (Vazyme Biotech, China). A sample of 50 µl total volume was placed in a Thermocycler using the following program: 72 °C for 3 min; 98 °C for 30 s; 17 cycles of 98 °C for 15 s, 60 °C for 30 s and 72 °C for 30 s; 72 °C for 5 min and hold at 4 °C. For PCR products purification, 1.2 × volumes of VAHTS DNA Clean Beads (Vazyme Biotech, China) were added and incubated at room temperature for 10 min. Libraries were washed twice with 80% ethanol and eluted in 22 µl of ddH2O.

Sequencing was performed on an Illumina NovaSeq platform and 150-bp paired-end reads were generated. All raw sequence data were quality trimmed to a minimum phred score of 20 using Cutadapt. All clean reads were qualified by FastQC and then paired-end aligned to the GCRh38 primary assembled human genome using Alignment via Burrows-Wheeler Transformation (BWA) version 0.7.15-r1140 with default parameters. Sequence tags were aligned to the genome and then subsequently analyzed by MACS2 software version 2.2.6 to detect genomic regions enriched for multiple overlapping DNA fragments (peaks) that we considered to be putative binding sites. Peaks with a false discovery rate lower than 5% were saved to detect chromosomal regions for further analyses. Visualization of peak distribution along genomic regions of interested genes was performed with IGV.

2.10. In vivo cell-derived xenograft experiments

For cell-derived xenograft experiments, five-week-old female nude mice were used. All mice were purchased from Beijing HFK Bioscience Co., LTD (Beijing China) and maintained under specific pathogen-free conditions and provided with sterile food and water. 1×10^6 stably infected NUGC3 cells resuspended in 100 µl PBS were subcutaneously injected into the flanks of nude mice. Following implantation, the mice were monitored by caliper once per week and tumor volumes were calculated using the formula (length × $width^2$)/2. Once the tumor reached ~150 mm^3 of volume, mice were treated orally daily with olaparib (50 mg/kg), AZD6738 (25 mg/kg). AZD6738 was given 1 h after administration of olaparib. Mice were monitored for tumor growth and overall health every three days. Once the tumor size reached 2000 mm^3, mice were euthanized. All animal testing and research were conducted according to approved protocol by Institutional Animal Care and Use Committee of the State Key Laboratory of Proteomics (Beijing).

2.11. Data analysis of proteomic raw file

MS raw files were processed with the Firmiana proteomics workstation [21]. Briefly, raw files were searched against the NCBI human Refseq protein database (released on 04–07–2013, 32,015 entries) in Mascot search engine (version 2.3, Matrix Science Inc.). The mass tolerances were 20 ppm for precursor and 50 mmu or 0.5 Da for product ions collected either by Fusion, respectively. The proteolytic cleavage sites are KR. Up to two missed cleavages were allowed. The database searching considered cysteine carbamidomethylation as a fixed modification and Acetyl (Protein N-term), oxidation of methionine as variable modifications. All identified peptides were quantified in Firmiana with peak areas derived from their MS1 intensity. Peptide FDR was adjusted to 1%. In the analysis of global proteomes, three or more high-confidence peptides (mascot ion score > 20) were required for protein identification, and also proteins with two high-confidence peptides (mascot ion score > 20) were included when any of these two peptides belongs to unique peptide. To achieve protein quantification, we used a label-free, intensity-based absolute quantification (iBAQ) approach [22]. The fraction of total (FOT), calculated by a protein's iBAQ divided by total iBAQ of all identified proteins in one experiment, was used to represent the normalized abundance of a protein across experiments. For easy representation, the FOT was then multiplied by 10^5 to obtain iFOT [23]. Missing values were substituted with zeros.

2.12. Quantification and statistical analysis

Principle component analysis, correlation analysis and Kaplan-Meier survival analysis were performed in R program. Statistical analysis was performed by the Student's t-test for two groups and by analysis of variance for multiple groups. *P* value lower than 0.05 was seen as significant.

3. Results

3.1. Proteome profiling of gastric cancer cell lines with differential PARP inhibitor sensitivity

We treated 12 gastric cancer cell lines with olaparib at a series of concentrations to investigate the sensitivity of gastric cancer cells to PARPi. Based on IC50 to olaparib, these cell lines were divided into insensitive group and sensitive group besides excluded MKN74 with an IC50 greater than 200 µM. In the sensitive group, IC50 of 6 cell lines ranged from 1.89 to 11.69 µM while it was greater than 30 µM in the insensitive group (Fig. 1A).

To explore the proteins responsible for discriminating two groups with different sensitivity, we performed label-free quantitative proteomics to the whole cell lysates of 12 cell lines with 3 biological replicates using 150 min high performance liquid chromatography separation along with single MS run. After filtering out gene products with less than 2 strict peptides (with Mascot ion score greater than 20) and those with 2 strict peptides but not unique, 7428 gene products were identified (Fig. S1A). Proteome quantification was performed with the previously reported iBAQ algorithm [22] followed by normalization to fraction of total (FOT). The dynamic range of iFOT was more than seven orders of magnitude (Fig. S1B).

Principle component analysis (PCA) and Pearson's correlation analysis of proteome revealed high repeatability among biological

replicates with correlation coefficients greater than 0.85 (Fig. S1C; Fig. S1D). Based on iFOT of quantified 7428 gene products, we observed few overall proteome differences between the insensitive group and the sensitive group as shown by PCA of 12 gastric cancer cell lines (Fig. 1B).

To discover effective biomarkers with high frequency in GC population, we selected 3695 gene products as candidates that were detected in more than five gastric cancer cell lines excluding MKN74 and with frequency of no less than 20% in our own proteome data of tumor tissues from 300 GC patients (data not published). Candidates' Pearson's correlation coefficients, each of which was calculated between indicated iFOT and IC50 of 11 gastric cancer cell lines to olaparib, ranged from −0.85 to 0.92 (Fig. 1C). Among these candidates, 127 gene products are involved in DNA repair pathway (R-HSA-73,894) based on Reactome database [24], and four gene products VCP (p97), PPP4C, COPS2 and TERF2IP, with absolute correlation coefficients greater than 0.7, obviously correlate with sensitivity to olaparib. VCP plays a role in protein degradation and is involved in DNA damage response as a BRCA1/-BARD1 cofactor [25]. PPP4C, as a protein phosphatase, forms PP4 complex with PPP4R2 and PPP4R3A, the complex specifically dephosphorylates gamma-H2AX phosphorylated on Ser-140 and is required for DNA double strand break repair [26]. PPP4C also catalyzes RPA2 dephosphorylation in response to DNA damage, which is an essential step for DNA repair allowing the efficient RPA2-mediated recruitment of RAD51 to chromatin [27]. COPS2, along with Ddb1 and Cullin4, implicate in nucleotide excision repair (NER) [28]. As for TERF2IP, also known as RAP1, was reported to be required for repression of homology-directed repair (HDR) and inhibition of PARP1 [29]. To sum up, this result of correlation analysis provides a credible list of protein candidates that affect sensitivity to olaparib. Considering PARP1 is the target protein of olaparib, we examined PARP1 expression levels in these cell lines and found that PARP1 protein with correlation coefficient of −0.046 was shown to poorly correlate with sensitivity to olaparib, consistent with previous reports (Fig. S2A)(6).

3.2. Correlation of MTA2 protein level with the GC cell sensitivity to PARP inhibitor and its analysis in tumor and nearby tissues from GC patients

Among proteins most positively correlated with GC cell sensitivity to olaparib, we noticed MTA2, which is a component of nucleosome remodeling deacetylase complex (NuRD complex) (Fig. 1C). We found that MTA2 expression level positively correlated with the cellular sensitivity to olaparib with correlation coefficient of −0.81, and consistently MTA2 levels in the sensitive group was significantly higher than those in the insensitive group (Fig. 1D; Fig. 1E). These results imply that higher MTA2 protein levels in GC cells increase their sensitivity to olaparib.

To further explore the application of MTA2 as a biomarker for olaparib in GC patients, we analyzed MTA2 expression in tumor and tumor-nearby tissues from GC patients. Based on analysis of a cohort of 300 GC patients by proteomics, MTA2 protein levels in tumor tissues are exceedingly higher than those in paired tumor nearby tissues from all GC patients (Fig. 1F; Fig. S2C-E). Furthermore, we observed a gradual increase of MTA2 levels in the superficial gastritis (SG)/chronic atrophic gastritis (CAG), intestinal metaplasia (IM)/ dysplasia (DYS) and GC tissues, which reflects the progress of GC (Fig. 1G, data not published). These results suggested that MTA2 continued to over express in stomach along with the pathological process. Kaplan-Meier survival analysis demonstrated that GC patients with high T/P ratio (tumor to the nearby tissue) of MTA2 (top 72.7%) had worse overall survival ($p = 0.022$) and worse disease-free survival ($p = 0.007$) compared to all others (Fig. S2B; Fig. 1H). Therefore, MTA2 expression is a prognostic indicator of poor prognosis for GC.

3.3. MTA2 enhances the GC cell sensitivity to olaparib by aggravating olaparib-induced replication stress

To further evaluate the potential application of MTA2 as a biomarker for olaparib in GC treatment, we chose MKN1 and NUGC3 cell lines with different sensitivity to olaparib as models, which possess distinguishing MTA2 protein levels (Fig. 1A). Knockdown of MTA2 in both MKN1 and NUGC3 cells promoted their resistance to olaparib, and the extent of resistance depended on the efficiency of knocking down using three separate siRNAs (Fig. 2A; Fig. S3A). To further validate the role of MTA2 in olaparib treatment, we performed dose course assay and colony formation assay on NUGC3 cells. Consistently, downregulation of MTA2 weakened the lethality of olaparib to GC cells in both assays (Fig. 2B; Fig. 2D). Consistently, overexpression of MTA2 in MKN1 cells correspondingly suppressed the growth of cancer cells together with olaparib in a dose-dependent manner (Fig. 2C; Fig. S3B). We observed that γH2AX, a DNA damage marker, was induced by olaparib treatment and increased gradually along with increasing concentrations as previously reported [7], however, the induction by olaparib was abrogated in MTA2-knockdown cells (Fig. 2E). These results confirmed the speculation that MTA2 accelerates olaparib-induced DNA damage and thus increases the sensitivity of GC cells to olaparib.

To further understand how MTA2 increases lethality of olaparib to GC cells, we performed interaction proteomics to Flag-MTA2 expressing or control AGS cells separately, and then analyzed proteins significantly enriched in Flag-MTA2 group (Fig. 3A). We found that seven proteins were involved in DNA replication progress according to previous reports, including H3F3C, SNRPE, DNMT1, WDHD1, RPA2, RECQL and HMGB3 [30,31]. It is known that olaparib-induced DNA lesions can cause replication-associated DNA damage by colliding with replication forks and triggering its collapse, which could consequently cause S-phase progression and G2/M checkpoint activation [32]. We therefore hypothesized that the increased lethality of olaparib by MTA2 was due to replication stress. To test our hypothesis, we conducted cell cycle assay in control or MTA2-knockdown MKN1 cells after 24 h olaparib or DMSO treatment. Olaparib treatment caused more cells arrest in G2/M phase dose-dependently as reported [33,34], while knockdown of MTA2 decreased cell population in G2/M phase under whether olaparib treatment or not (Fig. 3B). Observation in MKN1 cells with biological replicates and 23,132–87 cells further confirmed that MTA2 promotes arrest of cells in G2/M phase in synergy with olaparib (Fig. 3C; Fig. S3C). Because ataxia-telangiectasia mutated and Rad3-related (ATR) is known to be the kinase regulating S-phase progression and G2/M checkpoint activation in response to replication-associated DNA damage, we detected the ATR signaling in MTA2-knockdown cells after olaparib treatment by immunoblotting. Increased phosphorylation of CHK1 Ser345, CHK1 Ser317 and RPA32 Thr21 as substrates of ATR was observed following olaparib treatment, which correspondingly was abrogated by knockdown of MTA2 (Fig. 3D). These results suggested that MTA2 promotes sensitivity of olaparib to cancer cells through aggravating olaparib-induced replication stress which activates ATR to suppress replication stress-caused DNA damage.

3.4. Olaparib enhances the binding of MTA2 to replication origins

To investigate the biological function of MTA2 in aggravating olaparib-induced replication stress, we performed the Cleavage Under Targets and Tagmentation (CUT&Tag) assay to map 26,239 and 25,135 peaks for MTA2 in DMSO-treated and olaparib-treated MKN45 cells respectively. The sequence of 200-bp genomic regions with MTA2 summits as centers were subjected to motif-based sequence analysis tools MEME with default parameters, and the first five most significantly enriched motifs were shown (Table 1; Extended Data Table 1). In motifs enriched in DMSO-treated cells, G/C-rich motif as the most frequent of them with 7926 MTA2-binding sites (Table 1), was previously identified as an Origin G-rich Repeated Element (OGRE) that was overrepresented

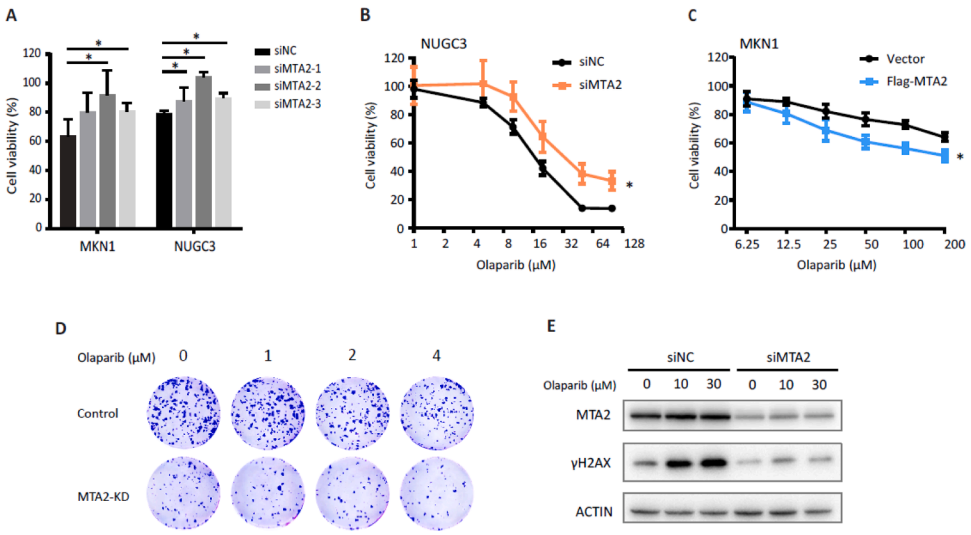

Fig. 2. MTA2 accelerates olaparib-induced DNA damage and enhances the GC cell sensitivity to olaparib. A Sensitivity of MKN1 and NUGC3 to olaparib after knocking down MTA2 or negative control. Statistical significance of the difference was analyzed using two-tailed unpaired Student's t tests, **p*-Value<0.05. B Proliferation of NUGC3 control or MTA2 knocking down cells with a concentration gradient of olaparib. C Proliferation of MKN1 control or MTA2 expressing cells with a concentration gradient of olaparib. Cells were examined by WST assay after 72-h olaparib treatment in B, C. Data are shown as mean ± SD, two-way analysis of variance (ANOVA), **p*-Value<0.05. D Clonogenic survival assay of the gastric cancer cell lines NUGC3 stably knocking down MTA2 or control GFP after olaparib (1 μM, 2 μM or 4 μM) treatment for 48 h. E Western blot analysis of γH2AX in MKN1 control or MTA2 knocking down cells treated with DMSO, 10 μM and 30 μM olaparib separately.

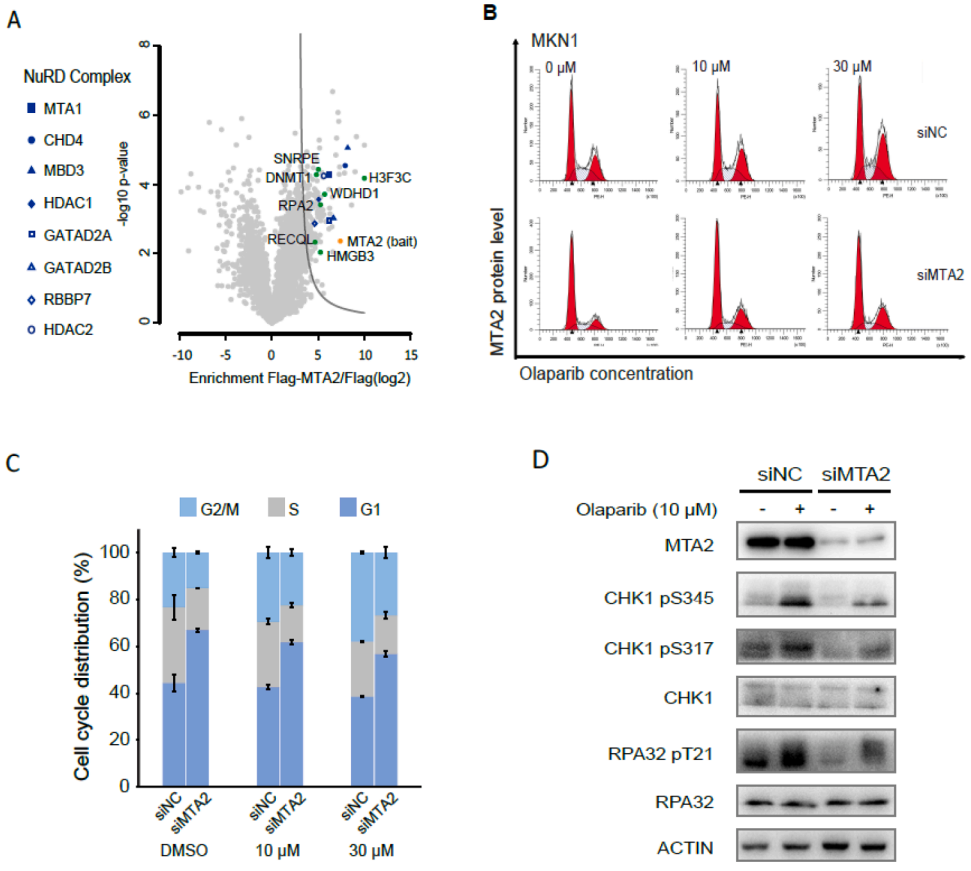

Fig. 3. MTA2 enhances olaparib-induced replication stress. A Interaction proteomics screen in AGS cells stably overexpressing Flag-tagged MTA2. Protein enrichment was calculated over the control AGS cells expressing Flag-tag alone and plotted against transformed t-test *p*-value. Gray line indicates significance threshold. The bait protein MTA2(orange), members of NuRD complex (blue) and replication-associated proteins(green) are highlighted. B, C Cell cycle profiles (B) and its statistical analysis (C) of high- or low- MTA2-expressing MKN1 cells treated with different concentrations of the PARPi olaparib (10 μM or 30 μM) for 24 h. Error bar represents standard deviation. D Western blot analysis of DDR proteins in MKN1 cell line with 10 μM olaparib treatment or DMSO. ACTIN is a loading control.

upstream of the initiation sites (IS) in Drosophila, mouse and human cells [35–37]. We also found another two replication origin-associated motifs, A/T-rich and TG repeats motifs, which together with G/C-rich motif were reported as specific genomic signatures to regulate origin localization in combination of specific chromatin environments [36]. Analysis of the genome-wide distribution of MTA2 in DMSO-treated cells showed that this protein preferentially binds to DNA sequence of specific genetic signatures associated with origins' regulation, indicating its strong correlation with DNA replication origins.

To further investigate how MTA2 varies in distribution along whole human genome in response to olaparib treatment, we compared peaks for MTA2 in olaparib-treated cells with those in untreated cells. Based on different peak analysis using MACS2, 171 down-regulated peaks and 1360 up-regulated peaks after olaparib treatment were identified (Fig. S4A). We next counted the number of up-regulated peaks and down-regulated peaks respectively in the regions of genomic features, including CpG islands (CGI), promoters (1 kb upstream), exons and intergenic regions. Of these different peaks, most up-regulated peaks were distributed in regions of CGI and exons, while down-regulated peaks were mainly located in intergenic regions (Fig. 4A). The

Table 1
MTA2-associated DNA motifs in DMSO-treated cells. The sequence of 200-bp genomic regions around the 26,239 MTA2 peak summits in DMSO-treated MKN45 cells were subjected to motif-based sequence analysis tools MEME with default parameters.

Motif ID	E-value	Sites	Logo
motif 1	1.1E-125	7926	
motif 2	1.8E-092	586	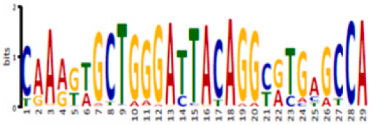
motif 3	1.5E-082	219	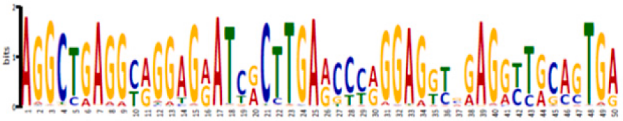
motif 4	2.6E-057	2179	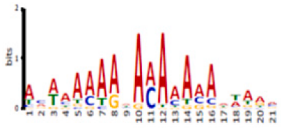
motif 5	2.4E-032	1043	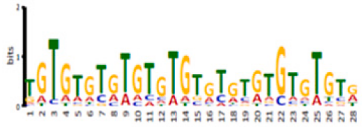

distribution of different peaks in regions of CGI along whole genome was shown in Fig. S4C. In addition, we observed a great overlap between distributions of CGI and MTA2 genome-widely in undisturbed cells (Fig. 4C). These results suggest that MTA2 preferentially binds to sequence within CGI regions, and the binding can be promoted by olaparib.

CGI are known to be fundamental elements in transcription regulation and imprinting in mammals controlled by methylation. Besides, we noticed that CGI sequences are associated with replication origins. A correlation of origins with unmethylated CGI was observed in the genome-scale studies in human and mouse cells [38–40]. In 2011, Cayrou et al. further revealed that CGI-related sequences could be seen as conserved determinants in a large part of mouse and Drosophila origins, regardless of their genomic position and methylation level [35]. Moreover, the binding of ORC complex to CGI was suggested by the same CGI properties of immunoprecipitated DNA fraction and that derived from short replication intermediates [41]. Because of these results, the presence of CGI can be used to assist in prediction and annotation of origins.

To observe the change of its distribution within CGI regions, we classified upregulated and downregulated peaks for MTA2 after olaparib treatment into three types, including spread, enhanced and unique types according to read density variations (Fig. 4D-F). Of 742 up-regulated peaks located in CGI regions, more than half belong to spread type, suggesting that olaparib accelerated progression of MTA2 along DNA sequence (Fig. 4B). In contrast, only 12 down-regulated peaks were located in CGI (Fig. S4B).

In conclusion, binding to origin-associated sequences and enrichment at CGI regions reveal a strong correlation of MTA2 with replication origins, which could be strengthened by olaparib.

3.5. MTA2 renders GC cells susceptible to combination of olaparib with ATR inhibitor

We hypothesized that MTA2's involvement in replication progress might make MTA2 sensitize cancer cells to ATR-inhibitor (ATRi). We therefore measured cell viability after ATRi AZD6738 (ceralasertib) treatment in MTA2-knockdown or control cells, and observed that knockdown of MTA2 as expected increased resistance of cancer cells to ATRi in both NUGC3 and MGC803 cells (Fig. 5A; Fig. 5B). Emerging evidence also suggest that ATRi could synergize with PARPi in both BRCA-deficient and BRCA-proficient backgrounds [33,42–44]. And given that MTA2 renders cancer cells sensitivity to olaparib and ATRi respectively, we further tested and found that olaparib combines synergistically with the ATRi, leading to more cell death in MTA2 high-expression backgrounds (Fig. 5C).

To further evaluate the in vivo efficacy of olaparib, AZD6738 and their combination, we established xenograft models by inoculating NUGC3-shGFP and NUGC3-shMTA2 cells subcutaneously into nude mice and treated them separately with olaparib, AZD6738 or in combination. Olaparib, AZD6738 and their combination all delayed tumor growth in MTA2-high xenografts compared with that in MTA2-low xenografts, with tumor growth inhibition rate of 26% to 5%, 37% to 20% and 54% to 23% separately (Fig. 5D; Fig. 5E). And the combination index of olaparib and AZD6738 in Fig. 5D is greater than 1 according to published methods [45–47], which indicates the combination effect of dual combination on tumor growth is a synergistic effect. These observations demonstrated a positive correlation between the level of MTA2 protein and sensitivity to olaparib, AZD6738 monotherapy or combined treatment in GC cell-derived xenograft mice, in accordance with what was observed in vitro results.

Overall, our data suggest that MTA2 protein could not only augment the lethality of olaparib and AZD6738 monotherapy to cancer cells but also enhance the suppression of cancer cells by combination of these two agents.

4. Discussion

In this study, we applied MS-based label-free quantitative proteomics to 12 gastric cancer cell lines and identified MTA2 as a biomarker of gastric cancer cells' greater sensitivity to olaparib. Using interactomics, functional assays and CUT&Tag assay, we found that MTA2

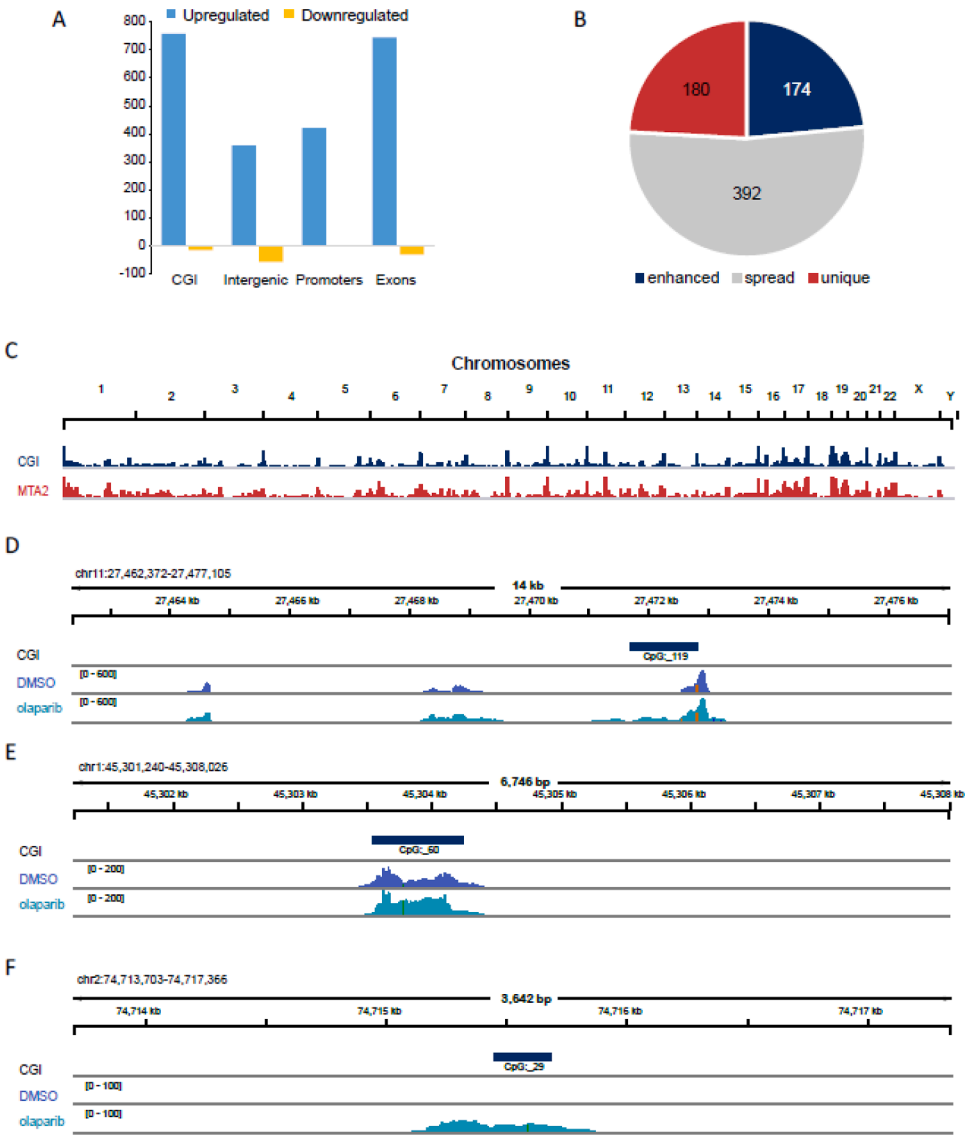

Fig. 4. MTA2 is involved in replication origin. A Counts of upregulated- and downregulated-peaks in olaparib-treated cells within 4 genome features. B Three types of up-regulated MTA2 peaks within CpG islands (CGI) regions after olaparib treatment and their respective counts. C Distribution of MTA2-binding DNA sequences (red) along whole human genomes. CGI distribution is in blue. D-F Spread, enhanced and unique types of upregulated peaks for MTA2 after olaparib treatment classified according to read density variations.

mechanistically aggravates olaparib-induced replication stress and is associated with replication origins. Accordingly, MTA2 synergizes with olaparib to enhance replication stress-associated DNA damage and to lead cancer cells to death. Here, we demonstrate that MTA2, which is proved to correlate with progress of GC, could serve as a biomarker to predict lethality of olaparib monotherapy or combination of olaparib and AZD6738 to cancer cells.

Mechanistically, MTA2 as a component of NuRD complex, is known to be involved in chromatin remodeling and thus affect transcriptional regulation, here we demonstrate its association with replication origins. We found that MTA2 proteins preferentially bind to sequences of three replication origin-associated motifs, which could characterize initiation sites together with chromatin modifications [36]. Replication initiates at a specific position downstream of the OGRE motif [35–37], which is the most enriched motif in our MEME analysis result. In consistent with our observation, Sergi et al. identified HDAC1-NuRD complex enriched at nascent DNA using isolation of proteins at nascent DNA technology [48]. In addition, Christo et al. found MTA2 and other three subunits of NuRD complex deposited in replication initiation activity fraction of Xenopus egg extracts and proved that NuRD complex initiated chromosomal DNA replication [49]. Notably, the pre-RC components ORC1–6, Cdt1, Cdc6, and most of MCM2–7 were not detected in the same fraction, indicating MTA2's involvement in replication origin 'licensing' step and its necessity in post-licensing step [49]. Given licensing step taking place during G1-phase, result of cell cycle analysis that reduction of MTA2 led cells to arrest in G1-phase agreed with our suggestion that MTA2 was associated with replication origins and might play a role in 'licensing' step. The specific molecular function of MTA2 associated with replication origin has not been explored in this article, it needs to be further studied in the future.

Notably, tumors with DNA replication stress can be suppressed by drugs targeting associated pathways or DNA damage repair. Along with sustained proliferation, replication rate and replication stress elevated in tumor cells, which has been seen as hallmarks of cancer [50,51]. As in the progress of GC, MTA2 level gradually increased possibly due to its involvement in DNA replication, and this implied the enhanced replication stress of stomach tumors. These tumor cells with enhanced replication stress are more dependent on DDR pathways for survival, which could be inhibited to suppress tumor growth. Correspondingly, we found that tumor cells with high MTA2 level are more sensitive to olaparib. DNA replication stress has also been reported to be a hallmark of renal medullary carcinomas and can be therapeutically targeted by olaparib [52]. Furthermore, inhibition of ATR pathway synergizes with PARP inhibition, leading cells to enhanced replication stress-induced genomic instability and abrogated DNA damage repair mechanism [33,43,53–55]. In agreement with previous reports, combination of

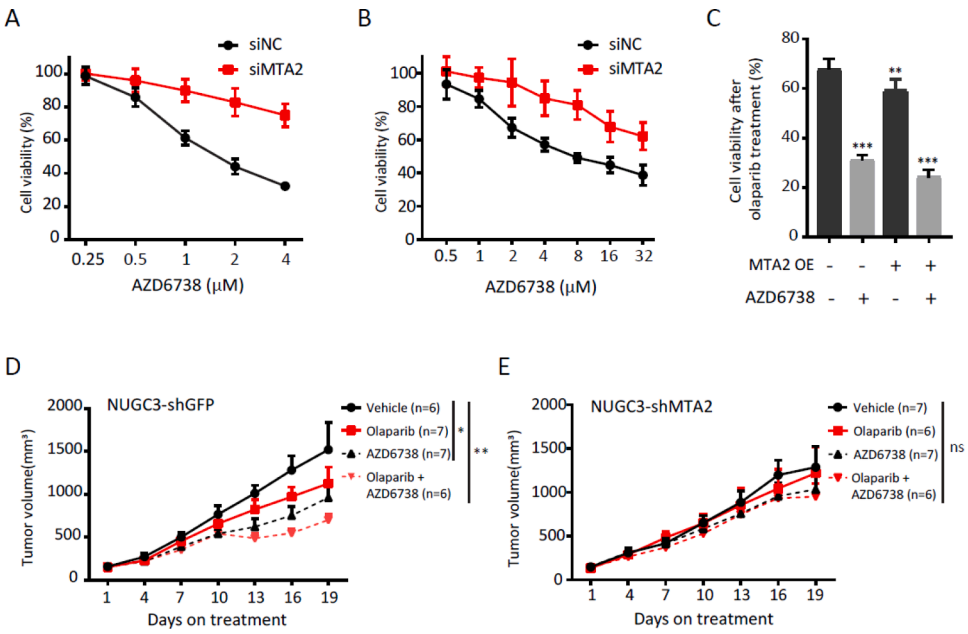

Fig. 5. MTA2 renders GC cells susceptible to ATRi and in combination with olaparib. A, B Proliferation of NUGC3 and MGC803 control or MTA2 knocking down cells with a concentration gradient of ATR inhibitor AZD6738. Cells were examined by WST assay after 24-h AZD6738 treatment. C Sensitivity of cells to 30 μM PARPi olaparib with MTA2 overexpression, 0.5 μM ATRi AZD6738 treatment or a combination of both. Statistical analysis used twotailed unpaired Student's t tests, **p*-Value<0.05, ***p*-Value<0.01, ****p*-Value<0.001. D, E Tumor growth curves depicting response of NUGC3-shGFP (D) and NUGC3-shMTA2 (E) subcutaneous tumors to the indicated treatment. Curves represent mean tumor volume (± SEM). Two-way ANOVA was used for statistical analysis. ns non-significant, **p*-Value<0.05, ***p*-Value<0.01, ****p*-Value<0.001.

ATRi AZD6738 and olaparib exhibited synthetic lethality in our study. Additional experimental evidence was further provided that MTA2 could promote the effect of synthetic lethality on cancer cells in our study. These results revealed that both intrinsically and extrinsically induced replication stress can be targeted to suppress cancer cell growth.

MTA2 could serve as a biomarker for olaparib to assist in patient selection, it was also an indicator of poor prognosis of GC for clinical application. GC is heterogeneous at both genetic and cellular levels [56], which may be one of the reasons that phase III study of olaparib did not meet its primary objective of showing a significant improvement in overall survival in patients with GC [57]. With MS-based proteomics providing new insights into biomarker screening and mechanistical understanding, we found a non-DDR associated factor MTA2 promoting olaparib to kill cancer cells. Furthermore, as an indicator of GC development, MTA2 expression was significantly elevated in GC tumor tissues comparing with nearby tissues of all three Lauren types (Fig. S2C-E). Therefore, it was much easier to detect MTA2 protein levels in tumor tissues, this is an advantage in the clinical application. These results implied that MTA2 could be used as a biomarker to select GC patients who may have worse prognosis but better response to olaparib monotherapy or in combination with ATRi.

Based on our results, MTA2 is expected to improve the efficacy of PARPi monotherapy for patients with advanced gastric cancer. In summary, continuing research on molecular mechanism and accumulating analysis of clinical data will deepen understanding of molecular changes after PARP inhibition and broaden views of therapeutical implication of PARPi.

CRediT authorship contribution statement

Jinwen Shi: Conceptualization, Methodology, Software, Validation, Formal analysis, Writing – original draft, Visualization. **Xiaofeng Zhang:** Validation. **Jin'e Li:** Software, Visualization. **Wenwen Huang:** Validation. **Yini Wang:** Writing – review & editing. **Yi Wang:** Conceptualization, Supervision. **Jun Qin:** Conceptualization, Writing – review & editing, Supervision, Funding acquisition.

Declaration of Competing Interest

The authors declare that they have no known competing financial interests or personal relationships that could have appeared to influence the work reported in this paper.

Supplementary materials

Supplementary material associated with this article can be found, in the online version, at doi:10.1016/j.tranon.2021.101167.

References

[1] F. Bray, J. Ferlay, I. Soerjomataram, R.L. Siegel, L.A. Torre, A. Jemal, Global cancer statistics 2018: GLOBOCAN estimates of incidence and mortality worldwide for 36 cancers in 185 countries, CA Cancer J. Clin. 68 (2018) 394–424.
[2] W. Xu, M.K. Beeharry, W. Liu, M. Yan, Z. Zhu, Preoperative Chemotherapy for Gastric Cancer: personal Interventions and Precision Medicine, Biomed. Res. Int. 2016 (2016), 3923585.
[3] C. Gravalos, A. Jimeno, HER2 in gastric cancer: a new prognostic factor and a novel therapeutic target, Ann. Oncol. 19 (2008) 1523–1529.
[4] C.M. Thallinger, M. Raderer, M. Hejna, Esophageal cancer: a critical evaluation of systemic second-line therapy, J. Clin. Oncol. 29 (2011) 4709–4714.
[5] F.Y. Feng, J.S. de Bono, M.A. Rubin, K.E. Knudsen, Chromatin to Clinic: the Molecular Rationale for PARP1 inhibitor function, Mol. Cell 58 (2015) 925–934.
[6] C. Bian, C. Zhang, T. Luo, A. Vyas, S.H. Chen, C. Liu, et al., NADP(+) is an endogenous PARP inhibitor in DNA damage response and tumor suppression, Nat. Commun. 10 (2019) 693.
[7] H.E. Bryant, N. Schultz, H.D. Thomas, K.M. Parker, D. Flower, E. Lopez, et al., Specific killing of BRCA2-deficient tumours with inhibitors of poly(ADP-ribose) polymerase, Nature 434 (2005) 913–917.
[8] H. Farmer, N. McCabe, C.J. Lord, A.N. Tutt, D.A. Johnson, T.B. Richardson, et al., Targeting the DNA repair defect in BRCA mutant cells as a therapeutic strategy, Nature 434 (2005) 917–921.
[9] P.G. Pilie, C. Tang, G.B. Mills, T.A. Yap, State-of-the-art strategies for targeting the DNA damage response in cancer, Nat. Rev. Clin. Oncol. 16 (2019) 81–104.
[10] G. Haddad, M.C. Saadé, R. Eid, F.G. Haddad, H.R. Kourie, PARP inhibitors: a tsunami of indications in different malignancies, Pharmacogenomics 21 (2020) 221–230.
[11] N.C. Turner, M.L. Telli, H.S. Rugo, A. Mailliez, J. Ettl, E.-.M. Grischke, et al., A phase II study of talazoparib after platinum or cytotoxic nonplatinum regimens in patients with advanced breast cancer and germline BRCA1/2 mutations (ABRAZO), Clin. Cancer Res. 25 (2019) 2717–2724.
[12] V. Gorbunova, J.T. Beck, R.D. Hofheinz, P. Garcia-Alfonso, M. Nechaeva, A. Cubillo Gracian, et al., A phase 2 randomised study of veliparib plus FOLFIRI±bevacizumab versus placebo plus FOLFIRI±bevacizumab in metastatic colorectal cancer, Br. J. Cancer 120 (2019) 183–189.
[13] A.F. Farago, B.Y. Yeap, M. Stanzione, Y.P. Hung, R.S. Heist, J.P. Marcoux, Combination Olaparib and Temozolomide in Relapsed Small-Cell Lung Cancer, Cancer Discov. 9 (2019) 1372–1387.
[14] Y.-.J. Bang, R.-.H. Xu, K. Chin, K.-.W. Lee, S.H. Park, S.Y. Rha, et al., Olaparib in combination with paclitaxel in patients with advanced gastric cancer who have progressed following first-line therapy (GOLD): a double-blind, randomised, placebo-controlled, phase 3 trial, Lancet Oncol. 18 (2017) 1637–1651.

[15] A. Gabrielson, A.A. Tesfaye, J.L. Marshall, M.J. Pishvaian, B. Smaglo, R. Jha, et al., Phase II study of temozolomide and veliparib combination therapy for sorafenib-refractory advanced hepatocellular carcinoma, Cancer Chemother. Pharmacol. 76 (2015) 1073–1079.
[16] C. Aghajanian, M.W. Sill, A.A. Secord, M.A. Powell, M. Steinhoff, Iniparib plus paclitaxel and carboplatin as initial treatment of advanced or recurrent uterine carcinosarcoma: a Gynecologic Oncology Group Study, Gynecol. Oncol. 126 (2012) 424–427.
[17] Y.J. Bang, S.A. Im, K.W. Lee, J.Y. Cho, E.K. Song, K.H. Lee, et al., Randomized, double-blind phase II trial with prospective classification by ATM protein level to evaluate the efficacy and tolerability of olaparib plus paclitaxel in patients with recurrent or metastatic gastric cancer, J. Clin. Oncol. 33 (2015) 3858–3865.
[18] S. Ge, X. Xia, C. Ding, B. Zhen, Q. Zhou, J. Feng, et al., A proteomic landscape of diffuse-type gastric cancer, Nat. Commun. 9 (2018) 1012.
[19] F. Coscia, E. Lengyel, J. Duraiswamy, B. Ashcroft, M. Bassani-Sternberg, M. Wierer, Multi-level proteomics identifies CT45 as a chemosensitivity mediator and immunotherapy target in ovarian cancer, Cell 175 (2018) 159–170, e16.
[20] Y. Chen, M. Leng, Y. Gao, D. Zhan, J.M. Choi, L. Song, et al., A cross-linking-aided immunoprecipitation/mass spectrometry workflow reveals extensive intracellular trafficking in time-resolved, signal-dependent epidermal growth factor receptor proteome, J. Proteome Res. 18 (2019) 3715–3730.
[21] J. Feng, C. Ding, N. Qiu, X. Ni, D. Zhan, W. Liu, et al., Firmiana: towards a one-stop proteomic cloud platform for data processing and analysis, Nat. Biotechnol. 35 (2017) 409–412.
[22] B. Schwanhausser, D. Busse, N. Li, G. Dittmar, J. Schuchhardt, J. Wolf, et al., Global quantification of mammalian gene expression control, Nature 473 (2011) 337–342.
[23] C. Zhang, Y. Chen, X. Mao, Y. Huang, S.Y. Jung, A. Jain, et al., A bioinformatic algorithm for analyzing cell signaling using temporal proteomic data, Proteomics 17 (2017).
[24] B. Jassal, L. Matthews, G. Viteri, C. Gong, P. Lorente, A. Fabregat, et al., The reactome pathway knowledgebase, Nucleic. Acids. Res. 48 (2020) D498–d503.
[25] A.N. Singh, J. Oehler, I. Torrecilla, S. Kilgas, S. Li, B. Vaz, et al., The p97-Ataxin 3 complex regulates homeostasis of the DNA damage response E3 ubiquitin ligase RNF8, EMBO J. 38 (2019), e102361.
[26] D. Chowdhury, X. Xu, X. Zhong, F. Ahmed, J. Zhong, J. Liao, A PP4-phosphatase complex dephosphorylates gamma-H2AX generated during DNA replication, Mol. Cell 31 (2008) 33–46.
[27] D.H. Lee, Y. Pan, S. Kanner, P. Sung, J.A. Borowiec, D. Chowdhury, A PP4 phosphatase complex dephosphorylates RPA2 to facilitate DNA repair via homologous recombination, Nat. Struct. Mol. Biol. 17 (2010) 365–372.
[28] C. Holmberg, O. Fleck, H.A. Hansen, C. Liu, R. Slaaby, A.M. Carr, et al., Ddb1 controls genome stability and meiosis in fission yeast, Genes Dev. 19 (2005) 853–862.
[29] R. Rai, Y. Chen, M. Lei, S. Chang, TRF2-RAP1 is required to protect telomeres from engaging in homologous recombination-mediated deletions and fusions, Nat. Commun. 7 (2016) 10881.
[30] C. Alabert, A. Groth, Chromatin replication and epigenome maintenance, Nat. Rev. Mol. Cell Biol. 13 (2012) 153–167.
[31] M. Fragkos, O. Ganier, P. Coulombe, M. Mechali, DNA replication origin activation in space and time, Nat. Rev. Mol. Cell Biol. 16 (2015) 360–374.
[32] J. Murai, S.Y. Huang, B.B. Das, A. Renaud, Y. Zhang, J.H. Doroshow, et al., Trapping of PARP1 and PARP2 by clinical PARP Inhibitors, Cancer Res. 72 (2012) 5588–5599.
[33] R.L. Lloyd, P.W.G. Wijnhoven, A. Ramos-Montoya, Z. Wilson, G. Illuzzi, K. Falenta, et al., Combined PARP and ATR inhibition potentiates genome instability and cell death in ATM-deficient cancer cells, Oncogene 39 (2020) 4869–4883.
[34] P. Jelinic, D.A. Levine, New insights into PARP inhibitors' effect on cell cycle and homology-directed DNA damage repair, Mol. Cancer Ther. 13 (2014) 1645–1654.
[35] C. Cayrou, P. Coulombe, A. Vigneron, S. Stanojcic, O. Ganier, I. Peiffer, et al., Genome-scale analysis of metazoan replication origins reveals their organization in specific but flexible sites defined by conserved features, Genome Res. 21 (2011) 1438–1449.
[36] C. Cayrou, B. Ballester, I. Peiffer, R. Fenouil, P. Coulombe, J.C. Andrau, et al., The chromatin environment shapes DNA replication origin organization and defines origin classes.pdf>, Genome Res. 25 (2015) 1873–1885.
[37] C. Cayrou, P. Coulombe, A. Puy, S. Rialle, N. Kaplan, E. Segal, et al., New insights into replication origin characteristics in metazoans, Cell Cycle 11 (2012) 658–667.
[38] J. Sequeira-Mendes, R. Díaz-Uriarte, A. Apedaile, D. Huntley, N. Brockdorff, M. Gómez, Transcription initiation activity sets replication origin efficiency in mammalian cells, PLos Genet. 5 (2009), e1000446.
[39] S. Delgado, M. Gómez, A. Bird, F. Antequera, Initiation of DNA replication at CpG islands in mammalian chromosomes, EMBO J. 17 (1998) 2426–2435.
[40] J.C. Cadoret, F. Meisch, V. Hassan-Zadeh, I. Luyten, C. Guillet, L. Duret, et al., Genome-wide studies highlight indirect links between human replication origins and gene regulation, Proc. Natl. Acad. Sci. U. S. A. 105 (2008) 15837–15842.
[41] E.M. Ladenburger, C. Keller, R. Knippers, Identification of a binding region for human origin recognition complex proteins 1 and 2 that coincides with an origin of DNA replication, Mol. Cell. Biol. 22 (2002) 1036–1048.
[42] H. Kim, E. George, R. Ragland, S. Rafail, R. Zhang, C. Krepler, et al., Targeting the ATR/CHK1 axis with PARP inhibition results in tumor regression in BRCA-mutant ovarian cancer models, Clin. Cancer Res. 23 (2017) 3097–3108.
[43] S.A. Yazinski, V. Comaills, R. Buisson, M.M. Genois, H.D. Nguyen, C.K. Ho, et al., ATR inhibition disrupts rewired homologous recombination and fork protection pathways in PARP inhibitor-resistant BRCA-deficient cancer cells, Genes Dev. 31 (2017) 318–332.
[44] B.T. Burgess, A.M. Anderson, J.R. McCorkle, J. Wu, F.R. Ueland, J.M. Kolesar, Olaparib Combined with an ATR or Chk1 inhibitor as a treatment strategy for acquired olaparib-resistant BRCA1 mutant ovarian cells, Diagnostics (Basel) 10 (2020).
[45] J.R. Zhou, L. Yu, Z. Mai, G.L. Blackburn, Combined inhibition of estrogen-dependent human breast carcinoma by soy and tea bioactive components in mice, Int. J. Cancer 108 (2004) 8–14.
[46] Y. Yokoyama, M. Dhanabal, A.W. Griffioen, V.P. Sukhatme, S. Ramakrishnan, Synergy between angiostatin and endostatin: inhibition of ovarian cancer growth, Cancer Res. 60 (2000) 2190–2196.
[47] T.C. Chou, P. Talalay, Quantitative analysis of dose-effect relationships: the combined effects of multiple drugs or enzyme inhibitors, Adv. Enzyme. Regul. 22 (1984) 27–55.
[48] S. Aranda, D. Rutishauser, P. Ernfors, Identification of a large protein network involved in epigenetic transmission in replicating DNA of embryonic stem cells, Nucleic. Acids. Res. 42 (2014) 6972–6986.
[49] C.P. Christov, K.S. Dingwell, M. Skehel, H.S. Wilkes, J.E. Sale, J.C. Smith, et al., A NuRD Complex from Xenopus laevis Eggs Is Essential for DNA Replication during Early Embryogenesis, Cell Rep. 22 (2018) 2265–2278.
[50] M. Macheret, T.D. Halazonetis, DNA replication stress as a hallmark of cancer, Annu. Rev. Pathol. 10 (2015) 425–448.
[51] J. Zhang, Q. Dai, D. Park, X. Deng, Targeting DNA replication stress for cancer therapy, Genes (Basel) 7 (2016).
[52] P. Msaouel, G.G. Malouf, X. Su, H. Yao, D.N. Tripathi, M. Soeung, et al., Comprehensive molecular characterization identifies distinct genomic and immune hallmarks of renal medullary carcinoma, Cancer Cell 37 (2020) 720. -34.e13.
[53] P. Gralewska, A. Gajek, A. Marczak, A. Rogalska, Participation of the ATR/CHK1 pathway in replicative stress targeted therapy of high-grade ovarian cancer, J. Hematol. Oncol. 13 (2020) 39.
[54] Y. Fang, D.J. McGrail, C. Sun, M. Labrie, X. Chen, D. Zhang, et al., Sequential therapy with PARP and WEE1 inhibitors minimizes toxicity while maintaining efficacy, Cancer Cell 35 (2019) 851–867, e7.
[55] M.K. Zeman, K.A. Cimprich, Causes and consequences of replication stress, Nat. Cell Biol. 16 (2014) 2–9.
[56] R. Wadhwa, S. Song, J.S. Lee, Y. Yao, Q. Wei, J.A. Ajani, Gastric cancer-molecular and clinical dimensions, Nat. Rev. Clin. Oncol. 10 (2013) 643–655.
[57] Y.J. Bang, R.H. Xu, K. Chin, K.W. Lee, S.H. Park, S.Y. Rha, et al., Olaparib in combination with paclitaxel in patients with advanced gastric cancer who have progressed following first-line therapy (GOLD): a double-blind, randomised, placebo-controlled, phase 3 trial, Lancet Oncol. 18 (2017) 1637–1651.